Effects of Neutral Impurity Scattering on the Low Field Electron Mobility in Bulk Silicon

Todd Hochwitz, Albert K. Henning

Thayer School of Engineering Dartmouth College Hanover, NH 03755

James Slinkman

IBM Microelectronics Essex Junction, VT 05452

Wilfried Hänsch

Siemens Components Incorporated 186 Wood Avenue Iselin, NJ 08830

September 8, 1994

Abstract

The Ridley Third Body Exclusion scattering formula for ionized impurities has been examined in a Monte Carlo simulation of low field bulk mobility for compensated *n*-type silicon. When the material is lightly doped ($N_d \leq 10^{16}$ cm^{-3}) and for lattice temperatures higher than 100 K the scattering formula results in an estimate for the bulk mobility that is comparable to experimental values. When the material is highly doped ($N_d > 10^{16}$ cm^{-3}) or the lattice temperature is below 100 K the Ridley scattering formula does not yield satisfactory results. Including neutral impurity scattering with the Ridley formula results in an excellent fit of the estimated electron mobility at room temperature for $N_d \leq 10^{18}$ cm^{-3}, and yields good results over the full range of lattice temperature, from 70 K to 300 K.

1 Introduction

Monte Carlo simulations have historically had difficulty with computing estimator values of carrier transport parameters in regions of semiconducting devices with low electric fields and high dopant concentrations. Thus, Monte Carlo simulations of electron transport in silicon most frequently compute transport estimator values in regions of device operation with high electric fields and low dopant concentrations. This work will show that the low electric field bulk mobility of electrons is not solely limited by ionized impurities, but also strongly influenced by neutral impurities. These low field results indicate that the nature of neutral impurity scattering may have an impact at higher electric fields, especially in cases where the doping density is high.

Most Monte Carlo simulators have been benchmarked against a particular set of experimental measurements [1, 2]. In these experiments, the applied electric fields are at least an order of magnitude lower than those encountered in critical regions of a Metal-Oxide-Semiconductor Field Effect Transistor (MOSFET). The silicon samples used have very low concentrations of dopants ($N_d \approx 5 \times 10^{12}$ cm^{-3}). As a result these measurements cannot suffice as the sole benchmark test for Monte Carlo simulations. Simulators benchmarked only against these experiments will have unknown validity to conditions of low field and

moderate doping (which occur in a MOSFET near the device source, and in the device channel), and to conditions of high field and moderate to heavy doping (which occur near and in the MOSFET drain).

Dopant levels in conventional MOSFETs exceed 10^{20} cm^{-3} in the source-drain regions, and are near 10^{17} cm^{-3} in the surface channel region. At such concentrations, ionized impurity scattering becomes significant under normal operating conditions. Ionized impurity scattering is typically treated as an elastic process, so only the momentum of charge carriers is changed. This mechanism may play an important role in the real space distribution of carriers in the channel of a device. An accurate simulator should thus predict low field bulk mobility consistent with available experimental values, as a function of both doping concentration and lattice temperature. Since the fraction of dopants which are ionized is also a function of these parameters, as a byproduct the simulator will account for the density of neutral, as well as ionized, impurities.

Conventional transport theory presumes that impurity scattering is negligible at higher electric fields, compared to phonon mechanisms. High field transport may, however, be affected by impurity scattering since the *neutral* impurity scattering rates in silicon can be comparable to the peak phonon scattering rates. From Figure 8.7 of [3], the peak scattering rate for phonons in silicon is roughly 2×10^{14} s^{-1} at an energy of 1.75 eV. At 1 eV the

total phonon scattering rate falls off to 8×10^{13} s^{-1}. With a dopant density of 10^{19} cm^{-3} in silicon, the scattering rate due to neutral impurities (from the model we present in this manuscript) at 1 eV is 9×10^{13} s^{-1}. Qualitatively, this implies neutral impurity scattering should be considered in the source, channel and drain regions of MOSFETs in order to properly model the transport physics.

The lack of sufficient high field measurements necessitates the successful simulation of low field transport for a variety of dopant concentrations and lattice temperatures. The success is determined by the strength of comparison between the simulation results and available measurements. A phenomenological model for the transport mobility in silicon at room temperature as a function of dopant density and electric field has been derived [4] and used for prediction in the literature [5]. These predictions are inconsistent with published low temperature experimental data [6]. The discrepancy may be attributed to mobility variation as a function of temperature, problems in inferring the mobility from current-based measurements, or the lack of inclusion of appropriate scattering mechanisms in the phenomenological model. Given this discrepancy and accompanying uncertainty over its source, we first seek to validate our Monte Carlo simulations against the available low field experimental data.

Theoretical models for ionized impurity scattering have been proposed by Brooks and

Herring [7], Conwell and Weisskopf [8], Samoilovich [9], Sclar [10], and Ridley [11]. Most experimental works focus on the Brooks–Herring theory for analyzing carrier mobilities. It has been reported that this theory is consistent with experimental results for lightly doped materials and higher temperatures [12, 13, 14], but overestimates the electron mobility at lower lattice temperatures and in highly doped material. The discrepancy has been attributed to electron-electron scattering [12], neutral impurities [13, 14], or electron-plasmon interactions [15].

There is evidence that neutral impurity scattering plays a significant role in semiconductors other than silicon. Blakemore performed studies of the effects of neutral Hg acceptors on the mobility of holes in germanium [16]. At low temperatures neutral impurity scattering had a detectable effect on the hole mobility. Blakemore determined that at very low lattice temperatures Hg^0 centers accounted for 35% of the heavy hole scattering, and 75% of the light hole scattering, in material doped with an acceptor concentration of $N_a \approx 10^{15}$ cm^{-3}. The scattering efficiency of Hg, a deep energy level divalent acceptor, is predicted to be 40% as strong as that of a shallow monovalent acceptor or donor [16]. Since conventional dopants in silicon are monovalent acceptors or donors, neutral impurity scattering may play a significant role in carrier transport. This is especially true for devices operating at lower lattice temperatures or when a significant number of the dopants are

un-ionized.

Norton, Braggins and Levinstein determined that for silicon, scattering via neutral impurities should affect electron mobilities significantly when $N_d \geq 10^{17}$ cm^{-3}, and at low temperatures [13]. The theoretical models used indicated that at 300 K neutral impurity scattering was twice as strong as ionized impurity scattering in a sample of silicon doped with phosphorus to a concentration of 3×10^{17} cm^{-3}.

To test the accuracy of the low field bulk mobility estimated by our Monte Carlo simulator, we have compared simulation results with published measurements [13]. The wide range of temperatures, dopant materials and doping concentrations examined in [13] provides the experimental foundation we require in order to validate our Monte Carlo simulator.

2 Monte Carlo Models

For this work one sampling electron was tracked in bulk silicon for an extended period of time under the application of a constant electric field. Scattering by intravalley acoustic phonons was treated inelastically. Intravalley optical phonon scattering (polar and non-polar) and impact ionization were turned off. Both *f*- and *g*-type intervalley phonon scattering were included.

The formulae used for acoustic and optical phonon scattering rates are the same as

described by Jacoboni and Reggiani [17]. With one exception, the parameters used for the coupling constants and phonon temperatures are the same. We found that a deformation potential of 4 eV/cm resulted in a better match of the drift velocity versus applied electric field.

Each of the six primary conduction valleys in silicon was explicitly included in modeling the conduction band. Since we were primarily concerned with the low field bulk mobility we could approximate the band structure of silicon with a simple ellipsoidal, nonparabolic formula relating the carrier energy to its mass and momentum wavevector as shown in Equation (1)

$$\gamma(\epsilon) = \epsilon\,(1 + \alpha\epsilon) = \frac{\hbar^2}{2m_o}\left(\frac{{k_l}^2}{m_l} + \frac{{k_{t_1}}^2}{m_{t_1}} + \frac{{k_{t_2}}^2}{m_{t_2}}\right) \tag{1}$$

where $\gamma(\epsilon)$ is the nonparabolic carrier energy, ϵ is the carrier energy, α is the nonparabolicity factor, $\hbar$ is Planck's constant divided by 2π, m_o is the mass of a free electron, m_l, m_{t1}, m_{t2} are the longitudinal and transverse effective masses, and k_l, k_{t1}, k_{t2} are the carrier wavevectors. For this work we used effective mass values of $m_l = 0.9163$, $m_t = 0.1905$, and a nonparabolicity factor of $\alpha = 0.5$ eV^{-1}.

The basis for the Ridley Third Body Exclusion scattering rate is a transport form of the Brooks–Herring formula that has been used in the experimental works cited earlier for describing the scattering rate. That formula contains a logarithmic term similar to

the Conwell–Weisskopf formula which arises from the integration over the scattering angle, and is presented here as Equation (2)

$$\frac{1}{\tau_{BH}} = \frac{N_I Z^2 e^4 (1+2\alpha\epsilon)}{32\sqrt{2m_g}\,\pi\,\kappa^2(\gamma(\epsilon))^{3/2}}\left[\ln(1+b) - \frac{b}{1+b}\right] \tag{2}$$

$$b = \frac{8m_g\gamma(\epsilon)}{\hbar^2\beta_{\mathrm{s}}^2} \tag{3}$$

$$\beta_{\mathrm{s}}^2 = \frac{ne^2}{\kappa k_B T} \tag{4}$$

$$\epsilon_\beta = \frac{\hbar^2\beta_{\mathrm{s}}^2}{2m_g} \tag{5}$$

where N_I is the total density of ionized impurities, Z is the valence of the ionized impurities, e is the electronic charge, κ is the dielectric constant of the material, ϵ_β is the effective screening energy, m_g is the density-of-states effective mass, β_{s} is the characteristic inverse screening length, n is the density of free carriers, k_B is Boltzmann's constant, T is the lattice temperature, and b is a dimensionless ratio of the carrier energy to the effective screening energy.

We used this formulation of Brooks–Herring in conjunction with Ridley's theory to scale appropriately the ionized impurity scattering rate for lower carrier energies [11]. This modified scattering rate is given in Equation (6)

$$\frac{1}{\tau_{RTBE}} = \frac{N_I^{1/3}\sqrt{2\gamma(\epsilon)}}{(1+2\alpha\epsilon)\sqrt{m_g}}\left[1 - \exp\left(\frac{-(1+2\alpha\epsilon)\sqrt{m_g}}{N_I^{1/3}\sqrt{2\gamma(\epsilon)}}\frac{1}{\tau_{BH}}\right)\right] \tag{6}$$

We chose the transport scattering formula (Equation (2)) over the conventional collision scattering formula (Equation (2.45) in [18]) in order to remain consistent with experimental mobility measurements. This choice is also consistent with our use of the classical mobility formula, Equation (8), which can be seen by examining Figure 1. The use of the collision scattering formula ($\frac{1}{\tau_c}$) in conjunction with Equation (8) results in a mobility that is much lower than experimental measurements – the contribution from ionized impurity scattering is too large. The use of the transport scattering formula in conjunction with Equation (8) results in the proper estimation of low field mobility. This comparison of results using $\frac{1}{\tau_c}$ and $\frac{1}{\tau_{BH}}$ indicates that in order to compare Monte Carlo results against experimental data, one must be careful to use the appropriate transport models and evaluate the transport estimators in a consistent manner.

A variation of Erginsoy's neutral impurity scattering rate [19] was used for our simulations, and is presented here as Equation (7)

$$\frac{1}{\tau_{NI}} = \frac{20\kappa\hbar^3\eta N_N}{e^2 m_g m_c (1+2\alpha\epsilon)} \tag{7}$$

where η is a dimensionless fitting parameter, N_N is the total density of neutral impurities, and m_c is the conductivity effective mass.

This scattering rate is proportional to the density of neutral sites and inversely proportional to the density-of-states and conductivity effective masses of an electron in silicon.

The only temperature dependence comes from the density-of-states effective mass and the number of un-ionized dopants. There is some evidence of a temperature dependence in the neutral impurity scattering rate [13, 16, 20, 21, 22], but we did not take this dependence into account for this work. It has been predicted [22] that within the temperature range we examined, the Erginsoy equation should be valid.

The dimensionless factor η was used as a fitting parameter, adjusted until the low temperature mobility was matched. η is an empirical correction factor for the effective Bohr radius, which changes the scattering cross-section of the neutral impurity sites. Band nonparabolicity does not significantly affect the neutral impurity scattering rate for carrier energies less than ≈ 100 meV.

The standard selection rules were used in determining the electron state after scattering via phonons [23]. The scattering angles used for ionized impurity scattering were the same as published by others [24]. Neutral impurity scattering was treated as an isotropic scattering mechanism [25].

We used the formulae and information about the experimental samples presented in [13] to determine the density of ionized and neutral impurities. The only information we did not include in computing the density of free carriers was the $1S$-state splittings. We computed the free carrier and impurity densities over a wide temperature range for each type of

dopant material and density of compensating material with the equation they included in their work, which was a variation of the formula given by Putley [26].

These values were then fed into our Monte Carlo simulator, along with a lattice temperature and a constant electric field of 10 V/cm that was applied in the <110> direction as with the experiment described in [13]. We allowed one sampling electron to travel through a lattice for 50 ns, which resulted in at least 15,000 scattering events at low temperatures and roughly 100,000 scattering events at room temperature. The maximum free flight timestep was 10 fs and a self-scattering value of 10^{14} s^{-1} was used, which exceeded the largest scattering rate by a factor of 2. There was less statistical uncertainty in the estimated mean free flight time than in the mean drift velocity. Therefore the classical definition of mobility (Equation 29.28 of [27], for example) was used to determine the estimated mobility as shown in Equation (8)

$$<\mu> = \frac{e<\tau>}{m_g} \tag{8}$$

where $<\tau>$ is the electron mean free flight time in the direction of the applied field. The density-of-states, as opposed to conductivity, effective mass was used to remain consistent with the Herring-Vogt transformation used in determining the scattering rates.

The mean free flight time was determined by accumulating the amount of time the sampling electron spent in free flight between scattering events, and was divided by the

number of free flight segments.

3 Doping Dependence of Bulk Mobility

We first examined the estimated mobility as a function of dopant density at room temperature. The values used were taken from the experimental results of Table X of [13]. The initial simulation sets included phonon and ionized impurity scattering.

Figure 1 shows the estimated mobility as computed with the Monte Carlo simulator. The Ridley model was successful in estimating the electron mobility up to 5×10^{16} cm^{-3}. Above this doping concentration the model overestimated the electron mobilities, consistent with [13].

The next test sets were intended to examine the effects of neutral impurity scattering. The value of η in Equation (7) was set to 1.0. The same set of impurity and free carrier concentrations was used. Figure 2 shows the estimated mobilities. This time the match between simulation and experimental data was much better. Use of the Ridley model and Erginsoy equation resulted in an estimated mobility that was within 10% of the experimental values.

Figure 3 shows the effect the Erginsoy model has on the relative strengths of the scattering mechanisms. The results indicate that neutral impurity scattering dominates when included with the Ridley formula at a doping concentration of 5×10^{17} cm^{-3}, but does

not exceed the scattering due to ionized impurities until the doping concentration exceeds 3×10^{17} cm^{-3}, which is again consistent with the theoretical observations of [13].

As will be discussed in the next section, a value of $\eta = 1.0$ for the Erginsoy formula does not result in satisfactory mobility results at very low temperatures, where neutral impurity scattering again dominates. A value of $\eta = 0.2$ seemed to give favorable low temperature results. A third set of simulations was carried out with this reduced neutral impurity strength at 300 K to see what the effects were on mobility at room temperature. The resulting mobilities can be seen in Figure 4. The mobility curve lies between the estimated mobilities from the previous two simulation sets.

4 Temperature Dependence of Bulk Mobility

The variety of doping concentrations and species in [13] provide an excellent opportunity to study the low field mobility in bulk silicon as a function of concentration and temperature. We performed simulations on 8 of the 9 samples discussed in [13], but will concentrate our discussion on the results for three samples that had comparable donor densities.

The data from Table I in [13] was used in computing the density of free carriers, ionized impurities, and neutral impurities over lattice temperatures from 25 K to 300 K. For the first set of simulations these values were fed into our Monte Carlo simulator without neutral

impurity scattering ($\eta = 0$). The estimated mobilities for three of the samples are plotted in Figures 5, 6, and 7. The Ridley model yields good estimates while the lattice temperature is above 70 K.

As was shown in the previous section, the mobility estimator becomes less accurate as the doping density increases. The results for the three samples are consistent with this, with the heavier doped sample showing a larger error between the simulated and experimental results (Figure 7). At lower temperatures a significant portion of the dopants are inactive, which will result in greater scattering rates and hence a lower electron mobility. The activation energies given in [13] lead one to suspect that neutral impurity scattering would play a more dominant role for arsenic than either phosphorus or antimony, since arsenic's larger activation energy results in a larger density of neutral impurities (the following values are given in [13]: $E_d \approx 53$ meV for arsenic, $E_d \approx 45$ meV for phosphorus, and $E_d \approx 43$ meV for antimony).

The Monte Carlo simulator was next used to examine the effect of neutral impurities on the low field mobility, with $\eta = 1.0$. The results can be seen in Figures 8, 9, and 10. In all cases, neutral impurity scattering reduced the low temperature estimated mobility.

The results also indicate a difference in the mobility reduction due to the type of dopant. Full strength neutral impurity scattering reduces the low temperature mobility in

phosphorus and antimony doped silicon by a factor of 3 or 4, and in arsenic doped silicon by a factor of 2. This is consistent with the differences in activation energies. For a given lattice temperature, there will be fewer activated arsenic sites than phosphorus/antimony sites since the activation energy places it further "down" along the exponential tail of the distribution function. Since the slope of the distribution is larger for the lower energy phosphorus/antimony sites, changing the scaling factor η will have a larger impact on the relative scattering strengths for those sites than for the arsenic sites as the lattice temperature changes.

Even though neutral impurity scattering causes the low temperature mobility to show a saturation similar to the experimental data, it is suppressed too much in arsenic. We tried reducing the value of η from 1.0 down to 0.2. This brought the low temperature mobility back up to the experimentally observed values, but overestimated the values for the middle temperature ranges (Figure 11). As was mentioned earlier it has been proposed that neutral impurity scattering has a temperature dependence [13, 16, 20, 21, 22]. These results by no means prove that such a temperature dependence exists, but a temperature dependence for η would give a better mobility estimate, especially when the doping concentration exceeds $\approx 10^{16}$ cm^{-3}.

5 Discussion

The Ridley Third Body Exclusion model yields estimates for electron mobility comparable to experimental values in lightly doped materials when the lattice temperature is above 100 K. The Ridley model overestimates the electron mobility when the doping exceeds 5×10^{17} cm^{-3} at room temperature.

As a consequence, it is necessary to include neutral impurity scattering in order to estimate electron mobility under higher doping concentrations, or to predict the saturation in mobility seen at lower temperatures. Our results show a correlation between the type of dopant material and the strength of neutral impurity scattering, which we have tried to model with an adjustable parameter. The physical basis for this parameter requires further examination. The Bohr radius requires a correction as a function of doping density in addition to temperature, and also will be the subject of further study. It should be considered along with several other possible factors for the discrepancy seen at higher doping densities.

One recent study has examined the use of phase-shift analysis and the Friedel sum rule to supplement the Brooks–Herring theory [28]. The researchers were able to obtain a very good fit of the experimental electron mobility in highly doped materials by introducing a

phenomenological model which may implicitly incorporate the effects of neutral impurity scattering.

Previous Monte Carlo simulation of low field mobility in GaAs is consistent with our results [24]. There, the Ridley model of ionized impurity scattering was demonstrated to be superior to the Brooks-Herring model in predicting low field mobility versus dopant concentration at 300 K and 77 K. Still, simulations carried out in the absence of neutral impurity scattering overestimated mobility throughout the range of dopant concentration at 77 K, and at higher dopant concentrations ($\approx 10^{17} - 10^{18}$ cm^{-3}) at 300 K. Based on our results, we expect that incorporation of neutral impurity scattering would also improve predictions of mobility in GaAs.

Carrier-carrier scattering would reduce the mean flight time, which would in turn reduce the mobility of the carriers, when the density of free carriers was high. If η is arbitrarily set to full strength, then including neutral impurity scattering with carrier-carrier scattering would result in an estimated mobility lower than the experimental results. Therefore it seems likely that the value of η should lie somewhere between 0.2 and 1.0, depending upon the strength of carrier-carrier scattering.

Another study has examined the influence of the electron-plasmon interaction on the electron mobility [15]. The phenomenon comes into play at doping densities larger than

those that we have examined. The plasmon energy is ≈ 20 meV at a doping density of $n = 10^{18}\text{cm}^{-3}$, which is much lower in energy than the intervalley optical phonons. At higher doping densities the plasmon energy is equal to or exceeds that of the intervalley optical phonons, and should also be considered. We have ignored this possibility, but feel that it could play a role when looking at higher doping densities, and should be examined in addition to neutral impurity scattering.

It has been suggested that, at high electric fields, electron transport in silicon is dominated by the band structure [29], derived from an examination of the electron-phonon interaction and its effect on pseudopotentials. It has long been accepted that ionized impurity scattering has little bearing on high field transport, however. Our work demonstrates that neutral impurities cause large changes in transport at low electric fields, for mid-range and higher doping concentrations. To the extent that dopant densities just below, near, and above the Mott transition are likely to modify band structure as well as low field mobility, they may also modify high field transport, and so require further study.

6 Conclusions

We have examined impurity scattering mechanisms in silicon, and their effect on estimations of low field mobility. This examination has been undertaken through a comparison of Monte Carlo simulation of low electric field transport, and measurements of low field

mobility, as a function of temperature and dopant concentration. We have found the Ridley Third Body Exclusion model, combined with a necessary addition of neutral impurity scattering, predicts measured low field mobility over a wide range of temperature and doping concentration. The results suggest that MOSFET mobility models, used in device-level, drift-diffusion simulation of conduction in surface inversion channels, may be improved through the inclusion of both the Ridley and neutral impurity scattering models. Furthermore, the modulation of band structure which occurs in heavily doped regions of MOSFETs indicates that transport in these regions – even under conditions of high electric fields – may also be affected by impurities.

7 Acknowledgments

This research has been funded through a Shared University Research contract with IBM Microelectronics, Essex Junction, Vermont.

References

[1] C. Canali, G. Ottaviani, and A. Alberigi-Quaranta, J. Phys. Chem. Solids **32**, 1707 (1971).

[2] C. Canali, C. Jacoboni, F. Nava, G. Ottaviani, and A. Alberigi-Quaranta, Phys. Rev. B **12**, 2265 (1975).

[3] K. Hess, *Advanced Theory of Semiconductor Devices* (Prentice Hall, Englewood Cliffs, NJ, 1988).

[4] D. L. Scharfetter and H. K. Gummel, IEEE Trans. Elect. Dev. **ED-16**, 64 (1969).

[5] C. Jacoboni, C. Canali, G. Ottaviani, and A. Alberigi-Quaranta, Solid-St. Electron. **20**, 77 (1977).

[6] J. G. Nash and J. W. Holm-Kennedy, Phys. Rev. B **16**, 2834 (1977).

[7] H. Brooks, in *Advances in Electronics and Electron Physics*, edited by L. Marton (Academic, New York, 1955), Vol. 7, pp. 85–182.

[8] E. Conwell and V. F. Weisskopf, Phys. Rev. **77**, 388 (1950).

[9] A. G. Samoilovich, I. Y. Korenblit, I. V. Dakhovskii, and V. D. Iskra, Sov. Phys. – Solid State **3**, 2385 (1962).

[10] N. Sclar, Phys. Rev. **104**, 1548 (1956).

[11] B. K. Ridley, J. of Phys. C **10**, 1589 (1977).

[12] D. Long and J. Myers, Phys. Rev. **115**, 1107 (1959).

[13] P. Norton, T. Braggins, and H. Levinstein, Phys. Rev. B **8**, 5632 (1973).

[14] D. Brown and R. Bray, Phys. Rev. **127**, 1593 (1962).

[15] M. V. Fischetti, Phys. Rev. B **44**, 5527 (1991).

[16] J. S. Blakemore, Phys. Rev. B **22**, 743 (1980).

[17] C. Jacoboni and L. Reggiani, Rev. Mod. Phys. **55**, 645 (1983).

[18] W. Hänsch, *The Drift Diffusion Equation and its Applications in MOSFET Modeling* (Springer-Verlag, Wien, Austria, 1991).

[19] C. Erginsoy, Phys. Rev. **79**, 1013 (1950).

[20] N. Sclar, Phys. Rev. **104**, 1559 (1956).

[21] L. E. Blagosklonskaya, E. M. Gershenzon, Y. P. Ladyzhinskii, and A. P. Popova, Sov. Phys. Solid St. **10**, 2374 (1969).

[22] L. E. Blagosklonskaya, E. M. Gershenzon, Y. P. Ladyzhinskii, and A. P. Popova, Sov. Phys. Solid St. **11**, 2402 (1970).

[23] H. W. Streitwolf, Phys. Stat. Sol. **37**, K47 (1970).

[24] T. G. V. de Roer and F. P. Widdershoven, J. Appl. Phys. **59**, 813 (1986).

[25] T. Ohyama, K. Murase, and E. Otsuka, Phys. Lett. **28A**, 159 (1968).

[26] E. H. Putley, Proc. Phys. Soc. (London) **72**, 917 (1958).

[27] N. W. Ashcroft and N. D. Mermin, *Solid State Physics* (Holt, Rinehart and Winston, New York, NY, 1976).

[28] L. E. Kay and T.-W. Tang, J. Appl. Phys. **70**, 1475 (1991).

[29] P. D. Yoder, V. D. Natoli, and R. M. Martin, J. Appl. Phys. **73**, 4378 (1993).

8 Figure Captions

Figure 1: Estimated electron mobility at 300K with ionized impurity scattering but without neutral impurity scattering as a function of donor concentration. The figure also shows the need to use the proper scattering rate in conjunction with the estimator Equation (8).

Figure 2: Estimated electron mobility at 300K with both ionized and neutral impurity scattering as a function of donor concentration.

Figure 3: Relative scattering strengths at 300K with Ridley and Erginsoy models as a function of donor concentration.

Figure 4: Estimated electron mobility at 300K with both ionized and weaker neutral impurity scattering as a function of donor concentration.

Figure 5: Estimated electron mobility in antimony doped silicon with $\eta = 0.0$ as a function of lattice temperature.

Figure 6: Estimated electron mobility in arsenic doped silicon with $\eta = 0.0$ as a function of lattice temperature.

Figure 7: Estimated electron mobility in phosphorus doped silicon with $\eta = 0.0$ as a function of lattice temperature.

Figure 8: Estimated electron mobility in antimony doped silicon with $\eta = 1.0$ as a function of lattice temperature.

Figure 9: Estimated electron mobility in arsenic doped silicon with $\eta = 1.0$ as a function of lattice temperature.

Figure 10: Estimated electron mobility in phosphorus doped silicon with $\eta = 1.0$ as a function of lattice temperature.

Figure 11: Estimated electron mobility in arsenic doped silicon with $\eta = 0.2$ as a function of lattice temperature.

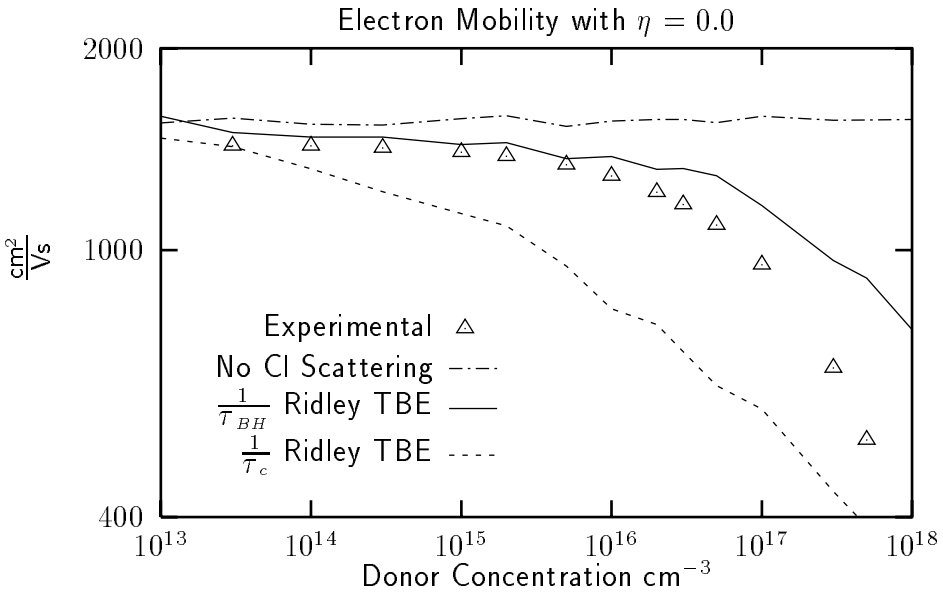

Figure 1: Hochwitz, Henning, Slinkman, Hänsch

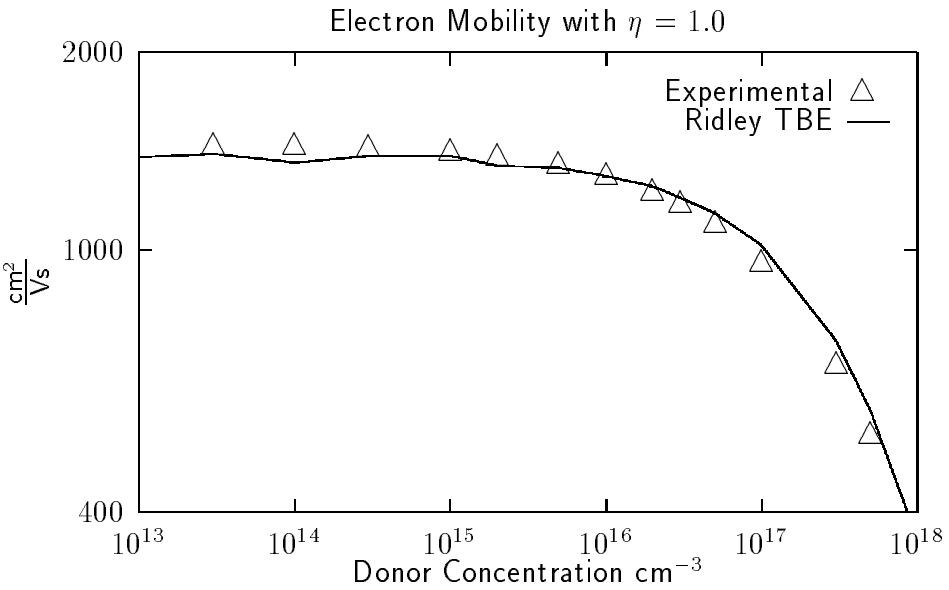

Figure 2: Hochwitz, Henning, Slinkman, Hänsch

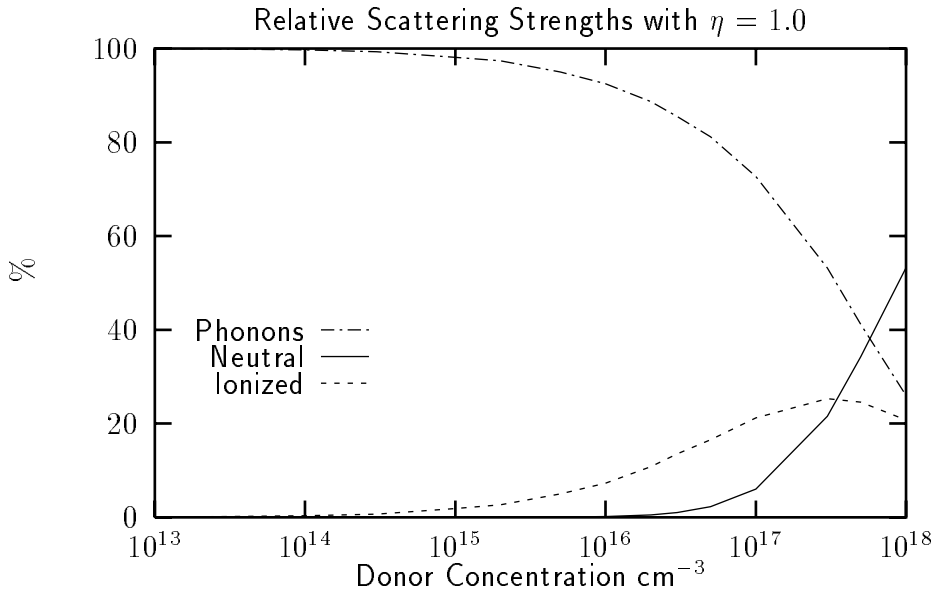

Figure 3: Hochwitz, Henning, Slinkman, Hänsch

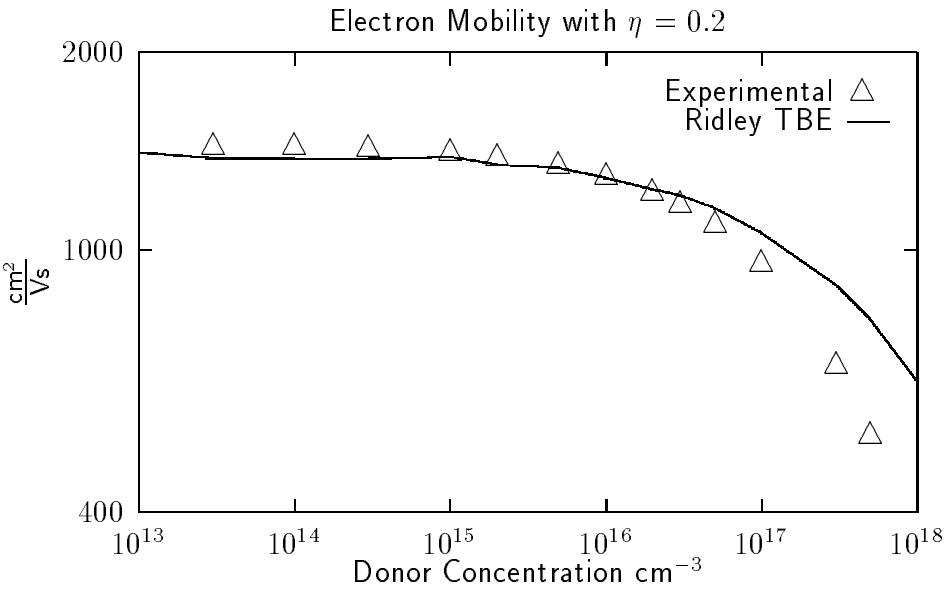

Figure 4: Hochwitz, Henning, Slinkman, Hänsch

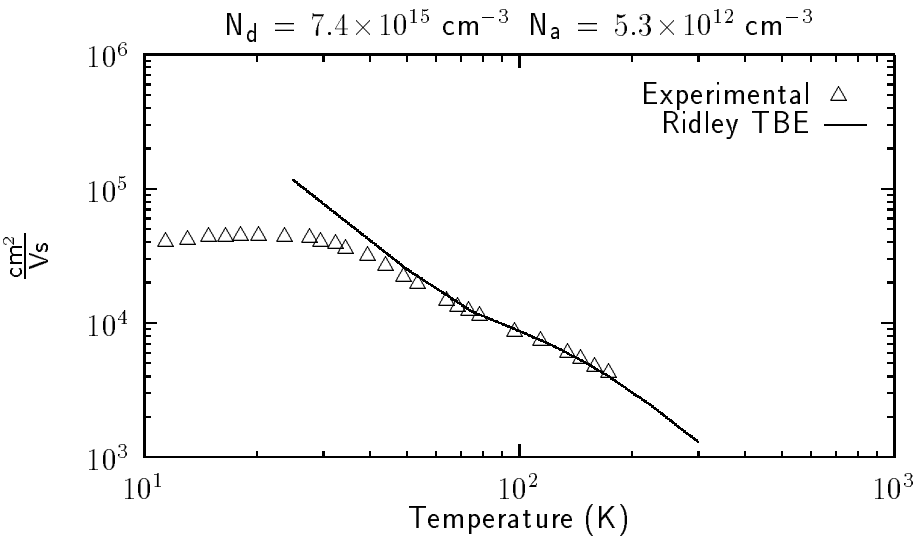

Figure 5: Hochwitz, Henning, Slinkman, Hänsch

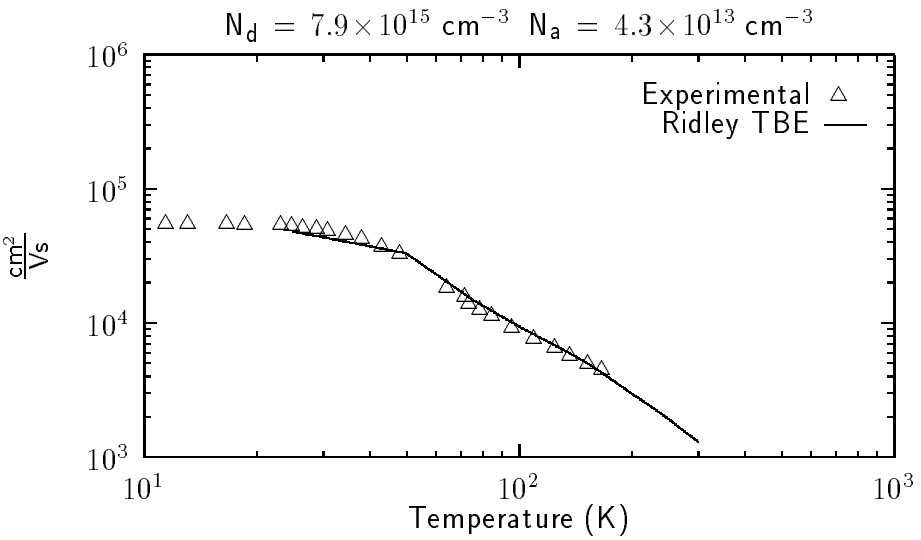

Figure 6: Hochwitz, Henning, Slinkman, Hänsch

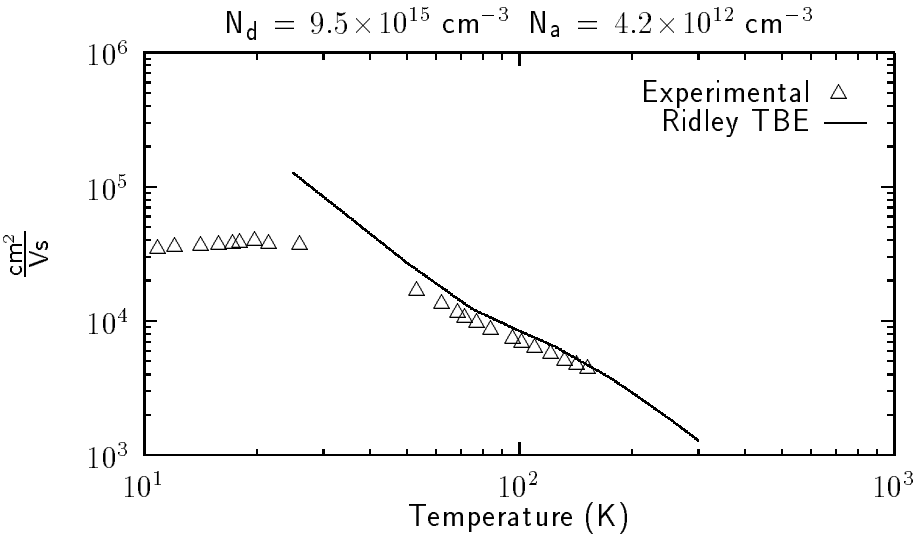

Figure 7: Hochwitz, Henning, Slinkman, Hänsch

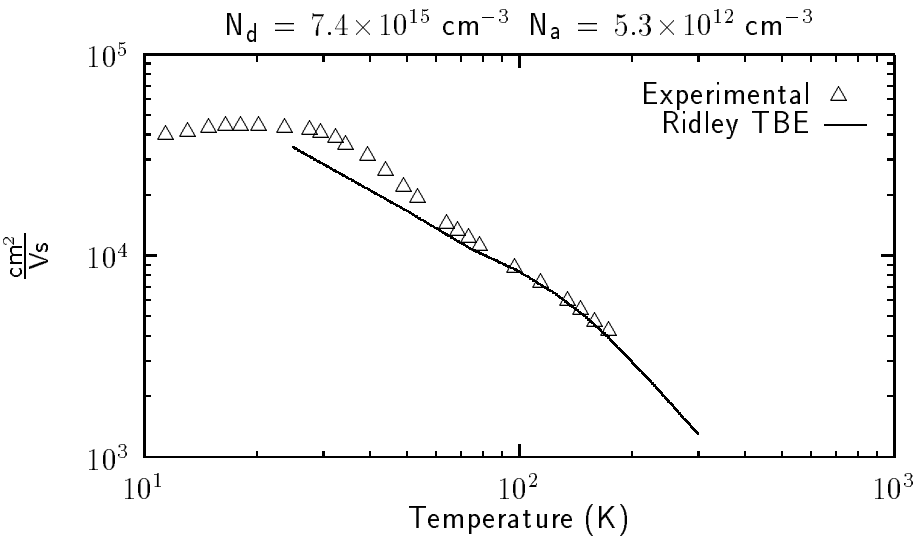

Figure 8: Hochwitz, Henning, Slinkman, Hänsch

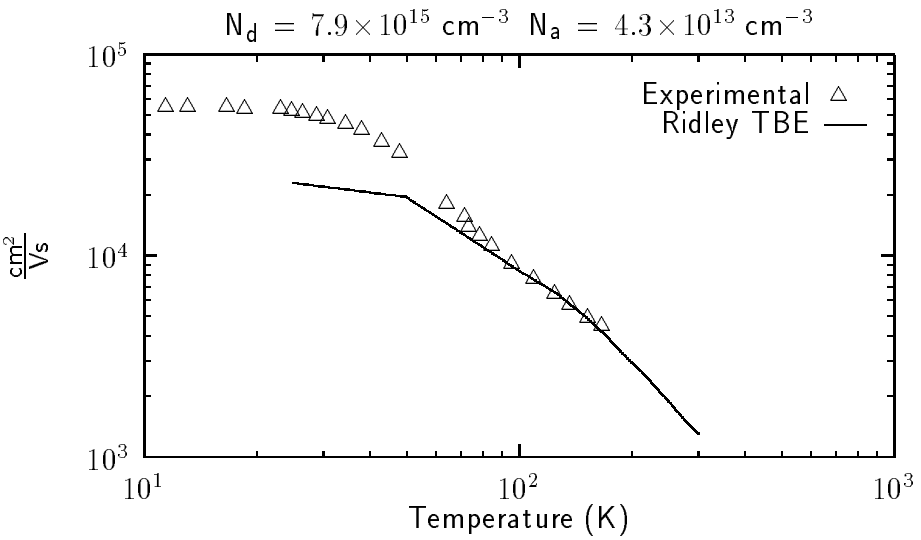

Figure 9: Hochwitz, Henning, Slinkman, Hänsch

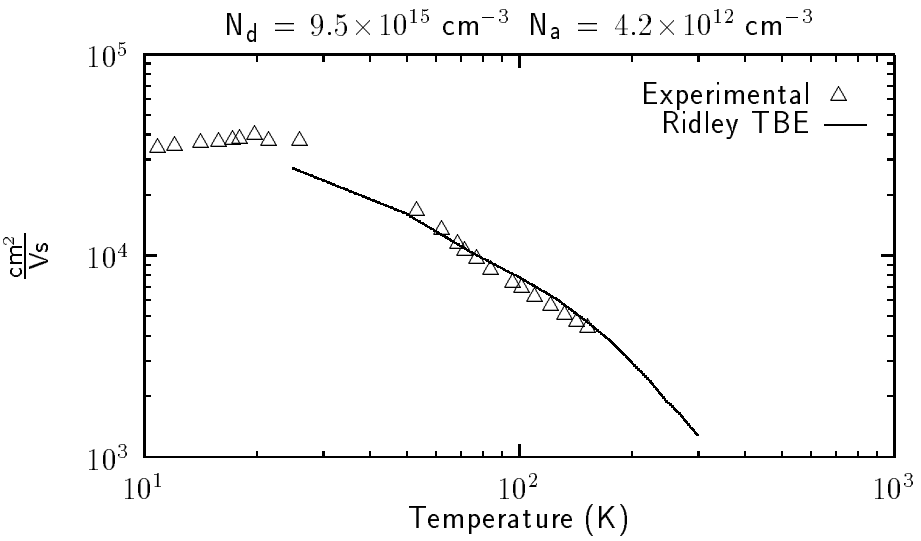

Figure 10: Hochwitz, Henning, Slinkman, Hänsch

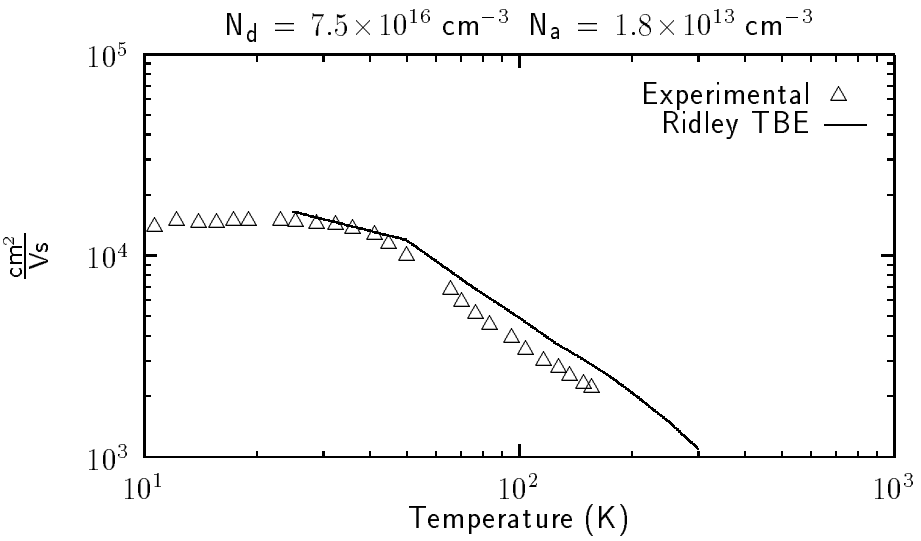

Figure 11: Hochwitz, Henning, Slinkman, Hänsch